EXTENDED PDF FORMAT
SPONSORED BY
usb
www.usbweb.com

Cassini Dust Measurements at Enceladus and Implications for the Origin of the E Ring

Frank Spahn, *et al.*

Science **311**, 1416 (2006);
DOI: 10.1126/science.1121375

The following resources related to this article are available online at www.sciencemag.org (this information is current as of October 24, 2007):

Updated information and services, including high-resolution figures, can be found in the online version of this article at:
http://www.sciencemag.org/cgi/content/full/311/5766/1416

Supporting Online Material can be found at:
http://www.sciencemag.org/cgi/content/full/311/5766/1416/DC1

A list of selected additional articles on the Science Web sites **related to this article** can be found at:
http://www.sciencemag.org/cgi/content/full/311/5766/1416#related-content

This article **cites 20 articles**, 7 of which can be accessed for free:
http://www.sciencemag.org/cgi/content/full/311/5766/1416#otherarticles

This article has been **cited by** 26 article(s) on the ISI Web of Science.

This article has been **cited by** 7 articles hosted by HighWire Press; see:
http://www.sciencemag.org/cgi/content/full/311/5766/1416#otherarticles

This article appears in the following **subject collections**:
Planetary Science
http://www.sciencemag.org/cgi/collection/planet_sci

Information about obtaining **reprints** of this article or about obtaining **permission to reproduce this article** in whole or in part can be found at:
http://www.sciencemag.org/about/permissions.dtl

Downloaded from www.sciencemag.org on October 24, 2007

Science (print ISSN 0036-8075; online ISSN 1095-9203) is published weekly, except the last week in December, by the American Association for the Advancement of Science, 1200 New York Avenue NW, Washington, DC 20005. Copyright 2006 by the American Association for the Advancement of Science; all rights reserved. The title *Science* is a registered trademark of AAAS.

REPORT

Cassini Dust Measurements at Enceladus and Implications for the Origin of the E Ring

Frank Spahn,[1] Jürgen Schmidt,[1]* Nicole Albers,[1] Marcel Hörning,[1] Martin Makuch,[1] Martin Seiß,[1] Sascha Kempf,[2] Ralf Srama,[2] Valeri Dikarev,[2,3] Stefan Helfert,[2] Georg Moragas-Klostermeyer,[2] Alexander V. Krivov,[3] Miodrag Sremčević,[5] Anthony J. Tuzzolino,[6] Thanasis Economou,[6] Eberhard Grün[2,4]

During Cassini's close flyby of Enceladus on 14 July 2005, the High Rate Detector of the Cosmic Dust Analyzer registered micron-sized dust particles enveloping this satellite. The dust impact rate peaked about 1 minute before the closest approach of the spacecraft to the moon. This asymmetric signature is consistent with a locally enhanced dust production in the south polar region of Enceladus. Other Cassini experiments revealed evidence for geophysical activities near Enceladus' south pole: a high surface temperature and a release of water gas. Production or release of dust particles related to these processes may provide the dominant source of Saturn's E ring.

The tenuous E ring is the outermost and largest ring in the saturnian system, consisting of particles with a peak size between 0.3 and 3 μm (*1*). The highest density of the E ring and its smallest vertical extent are both observed close to the orbit of Enceladus (*1*, *2*), which favors this moon as the main source of that faint ring. In situ dust measurements at Enceladus with the dust detector aboard the Cassini spacecraft offer the unique opportunity to learn about this satellite and about dust-production processes at its surface and, ultimately, to shed light on the origin of the E ring.

We report on measurements carried out with the High Rate Detector (HRD) of the Cosmic Dust Analyzer (CDA) during the flyby of Enceladus on 14 July 2005. The detector consists of two thin (28 μm and 6 μm) polyvenylidene fluoride sensors with cross sections of 50 cm^2 and 10 cm^2 (*3*). Here, we focus on the data collected by the 50-cm^2 sensor, which is sensitive for particles with a radius larger than 2 μm. An impacting hypervelocity grain changes the polarization in the sensor volume, resulting in a short, sharp pulse enabling the detector to register up to 10^4 dust impacts s^{-1} (*4*).

During the flyby, a significant increase in the count rate of dust particles was recorded about 10 min before to about 10 min after the closest approach of the spacecraft to the moon (Fig. 1). The peak count rate was 4 particles s^{-1} at 1 min before the closest approach. Similarly, the Cassini Ion and Neutral Mass Spectrometer (INMS) (*5*) detected water gas, also at a peak rate before the closest approach, albeit with a somewhat smaller offset of 30 s. This gas plume was also seen by the Ultraviolet Imaging Spectrograph (UVIS) (*6*) and, indirectly at an earlier flyby, by the magnetometer (*7*). The time difference between the rate peaks points to a decoupling of gas and dust shortly after both components are released from the satellite surface (*8*). A gas and dust source near the south pole is compatible with these premature maxima of the rates, because the spacecraft approached the moon from the south and came closest to Enceladus at a latitude of ~25°S [figure 1 of (*5*, *9*)]. In contrast, a dust cloud generated by micrometeoroid impacts, as was observed by the Galileo mission around the jovian moons (*10*), would lead to a peak rate directly at the closest approach.

The observed particle count rate constrains the production rate of particles at Enceladus, while the time offset of its maximum from the closest approach can be used to locate those regions on the moon's surface from which the particles originate. Comparing the data to theoretical models of dust production, we can estimate the relative contributions of alternative mechanisms of particle creation, yielding implications for the dominant source of the E-ring particles. Besides geophysical processes (*11*, *12*), micrometeoroid bombardment has been proposed as a particle-creation process (*13*). Two families of micrometeoroids are relevant at Enceladus, namely E-ring particles and interplanetary dust particles. The typically large velocities of such projectiles relative to the moon, from a few to tens of kilometers per second, make the impacts energetic enough to abundantly produce ejecta at the moon's surface and create a dust cloud (*10*, *14*). However, the detection of an anomalously high temperature (*9*) in the south polar region of Enceladus near elongated cracked fractures (*15*) (dubbed "tiger stripes") lends new support to the idea of E-ring dust particles created by cryovolcanism (ice volcanoes).

We have modeled the distributions of dust in the vicinity of Enceladus for cases of isotropic ejection of grains from the entire surface and for a localized dust source at the south pole of the moon (Fig. 1). These two cases correspond to the particle production by the impactor-ejecta mechanism and by geological processes at the south pole, respectively. Because the spacecraft's trajectory near the closest approach (168.2 km above the surface) lies well inside the Hill sphere (*16*) of gravitational influence of the moon [$r_h \sim 948$ km, compared with a radius of 252.1 km (*15*)], an analytical model for the dust cloud developed in (*17*), based on the two-body approximation, should give an adequate estimate (*18*). However, to account for the full three-body dynamics near the Hill scale, we have numerically simulated the dust configuration around the satellite for both source models. In the simulations, particle paths are integrated subject to Saturn's and Enceladus' gravity (*18*, *19*). In both simulations, 1 million particles are launched from the satellite's surface, with starting conditions that are plausible for particles created in an impactor-ejecta process (*20*, *21*). To simulate the impactor-ejecta source, the starting positions are chosen uniformly over the entire surface of the moon. The localized source is simulated with starting positions distributed uniformly in a circular area of an angular diameter of 30° centered at the south pole, which is on the order of the size of the hot region (*9*). The motion of the particles governed by the gravity of the planet and the satellite does not depend on the particles' mass or radius; thus, grains with different radii need not be distinguished in the simulations. Therefore, the size distribution in the model dust cloud near the moon derives from the particle size distribution assumed for the particle-creation process.

In the simulations, the impactor-ejecta process is found to generate a highly symmetric dust configuration in the vicinity of the satellite, as expected, so that the HRD on a flyby through this cloud would observe a maximal count rate directly at the closest approach (Fig. 1A). In contrast, the simulated dust ejection from the south pole source reproduces well the observed maximal count rate 1 min before the closest approach.

[1]Institut für Physik, Universität Potsdam, Am Neuen Palais 10, Haus 19, D-14469 Potsdam, Germany. [2]Max Planck Institut für Kernphysik, Saupfercheckweg 1, 69117 Heidelberg, Germany. [3]Astrophysikalisches Institut, Friedrich Schiller Universität, 07745 Jena, Germany. [4]Hawaii Institute of Geophysics and Planetology, University of Hawaii, Honolulu, HI 96822, USA. [5]Laboratory for Atmospheric and Space Physics, University of Colorado, Boulder, CO 80303, USA. [6]Laboratory for Astrophysics and Space Research, University of Chicago, Chicago, IL 60637, USA.

*Corresponding author: jschmidt@agnld.uni-potsdam.de

Downloaded from www.sciencemag.org on October 24, 2007

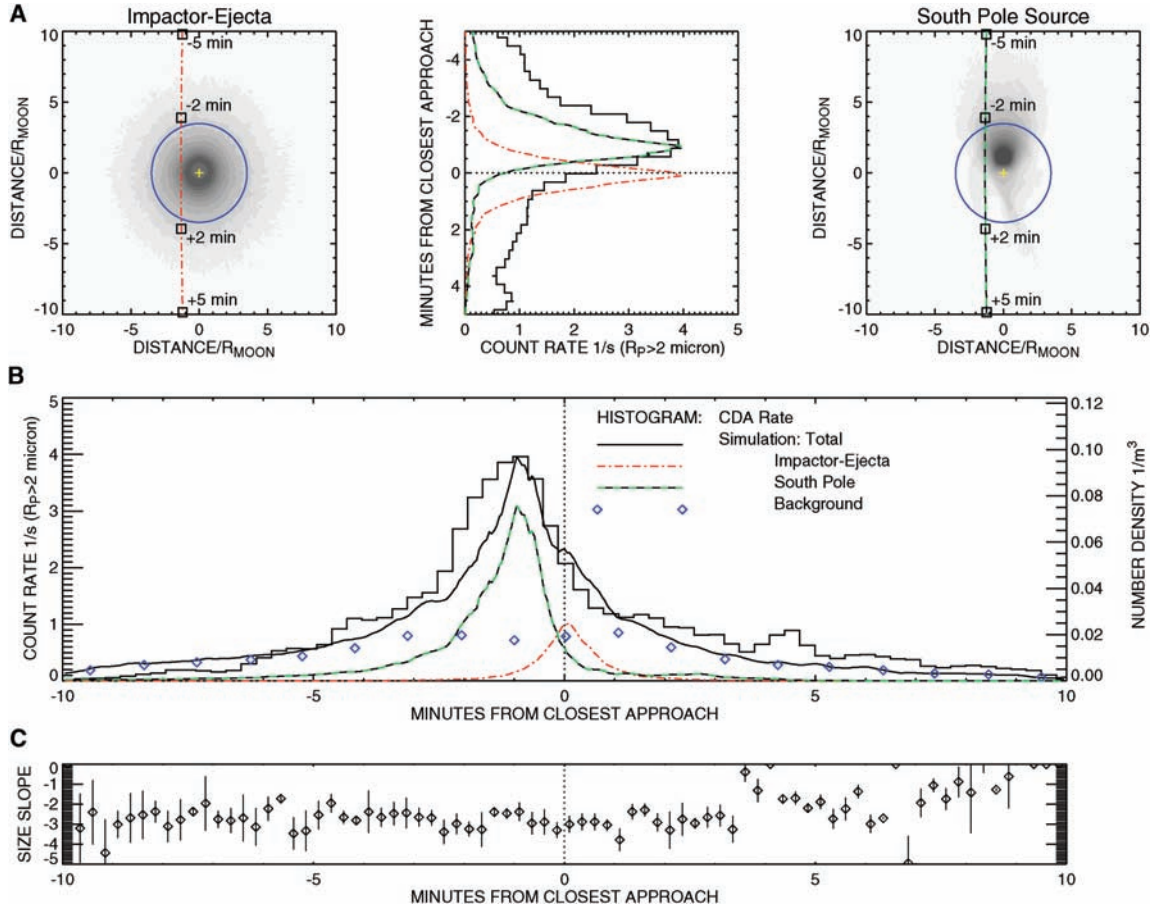

Fig. 1. Comparison of the CDA data to simulations. (**A**) Particle density in the plane of Cassini's trajectory estimated from simulations, darker shades referring to a higher density. The impactor-ejecta process (left) leads to a more symmetric dust cloud, whereas a localized source at the south pole of the moon (right) shows a strong asymmetry. Circles denote the intersection of the plane with the Hill sphere of gravitational influence, and the normal projection of the moon's center (not in that plane) is marked by a cross symbol. Cassini's trajectory is plotted as a dash-dotted or dashed line, respectively. The central plot shows the count rates predicted by the simulations computed along the actual spacecraft trajectory, both normalized to the peak rate of the data shown in histogram mode. (**B**) The sum of the rates derived from the two simulations and the simulated E-ring background, normalized to the observed peak rate. The maximal strength of the impactor-ejecta process relative to that of the south pole source is chosen in a way that no secondary peak develops in the combined rate near the closest approach. (**C**) The slopes of the differential size distribution $n\,(R_p) \propto R_p^{\alpha}$ versus time to the closest approach. The increase of α for $t > 4$ min is due to a maneuver of Cassini and the related change in the instrument's boresight.

Fitting combinations of both contributions with a consistent E-ring particle background to the data, and requiring that no second peak develops in the rate at the closest approach, we can estimate the maximal strength of the impactor-ejecta dust creation at Enceladus relative to that of the south pole source (Fig. 1B). From this fit (HRD data for $R_p > 2$ μm), we can infer the rate of particles larger than 2 μm emitted by the south pole source and escaping the moon's gravity to amount to 5×10^{12} particles s^{-1}, whereas the impactor-ejecta mechanism would produce at most 10^{12} such particles s^{-1}. These numbers correspond to an escaping mass of at least 0.2 kg s^{-1}, assuming $R_p = 2$ μm for all grains. For an extended size distribution, this rate may extend to kilograms per second. The E-ring particle background, which is naturally contained in the HRD data, has been simulated, following the motion of particles subject to gravity and perturbation forces (*18*, *19*), until they are lost in collisions with Enceladus, other E-ring moons, or the main rings. A self-consistent combination of the simulated dust populations is in reasonable agreement with the observed HRD rate (Fig. 1B).

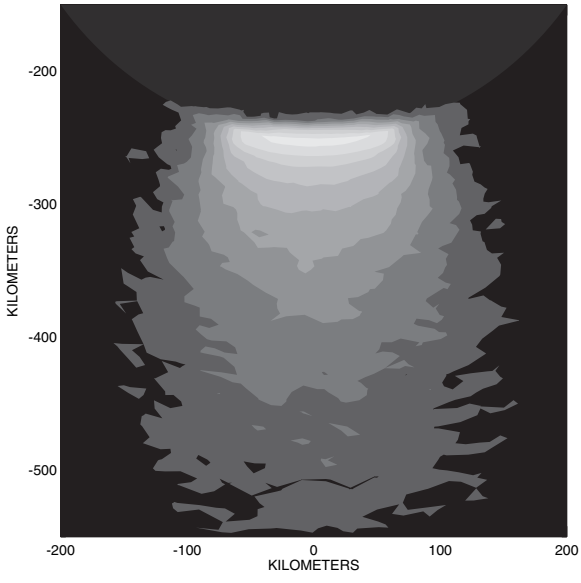

Fig. 2. Side view of a simulated dust plume at Enceladus' south pole. Contours of equal column particle density are shown in a Cartesian frame fixed at the center of the moon. The brightest contour denotes 10^7 particles per m^2, the column density dropping by one-half from level to level.

A differential particle size distribution inferred from the data of both HRD sensors fits to a power law $n\,(R_p) \propto R_p^{\alpha}$ with a slope $\alpha \sim -3$ that remains almost constant during the flyby (Fig. 1C). This near constance of the exponent indicates that the dynamics of larger grains is

Downloaded from www.sciencemag.org on October 24, 2007

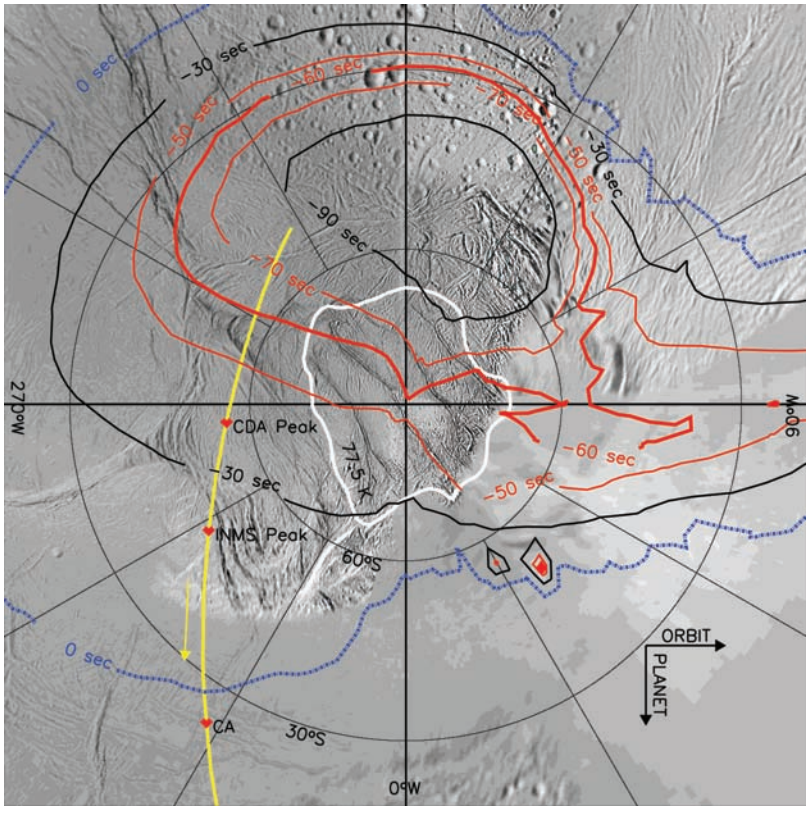

Fig. 3. Results of a series of simulations where the position of the source is varied systematically over the moon's surface. For each simulation, the particle count rate along the Cassini trajectory is computed. The contours of equal time offsets of the maximal count rate from the closest approach are plotted over a base map of Enceladus' south pole (*15*). The thick red line marks the contour of a –60-s offset of the maximal count rate, which was about the value observed by the CDA. Other contours correspond to offsets of –90, –70, –50, –30, and 0 s. The white line around the pole denotes the 77.5-K isotherm from the Composite Infrared Spectrometer (*9*). Cassini's ground track is shown in yellow, and the times of rate maxima of the CDA (–50 s) and INMS (–30 s) (*5*), as well as the closest approach (CA), are marked.

dominated by gravity. Such a power law is expected for an impactor-ejecta particle formation scenario (*20*). On the other hand, we showed that the south pole source should be the dominant source of particles. A possible explanation would be that the particles are formed in meteoroid impacts and lifted by south polar gas venting. However, an effective acceleration of grains in the gas plume seems implausible for the gas densities inferred from UVIS (*6*, *15*).

A side view of the dust configuration from the simulation of the south pole source is shown in Fig. 2, where the absolute numbers are fixed by HRD data at the closest approach. A similarly strong stratification of the dust density is evident in images of the dust plume (*15*). In the simulation, the stratification results basically from the power-law distribution of particle starting velocities (*21*).

To investigate the influence of the particle source location on the rate profile measured by HRD, we performed a series of about 2600 simulations, where the source position was systematically varied over the moon's surface. Here, we used 50,000 particles per simulation, employing for simplicity the initial conditions for the impactor-ejecta mechanism (*20*). For each source, we determined the time offset of the peak count rate to the closest approach for this flyby. In this way, we obtained a contour map of offset times over the moon's surface, which is plotted over an Image Science Subsystem base map (*15*) of the geologically active south pole region in Fig. 3. It was found that only a small part of the total surface of Enceladus can have sources that would match the actually observed offset of –1 min. Interestingly, the region of the tiger stripes (covering latitudes > 70°S) is indeed compatible with the data, yielding offsets from –50 to –70 s.

On the basis of simulations of the dust environment around Enceladus, we conclude that the Cassini CDA data of the Enceladus flyby on 14 July are compatible with a dust source in the south polar region of the moon. A particle ejection mechanism caused by hypervelocity micrometeoroid impacts alone cannot explain the data. New in situ measurements of Enceladus' dust cloud will be obtained during a flyby in 2008 at an altitude of only 100 km over 69°N.

References and Notes

1. P. D. Nicholson *et al.*, *Science* **272**, 509 (1996).
2. M. R. Showalter, J. N. Cuzzi, S. M. Larson, *Icarus* **94**, 451 (1991).
3. R. Srama *et al.*, *Space Sci. Rev.* **114**, 465 (2004).
4. This property of the HRD becomes crucial in regions of high particle density (parts of the E ring and in the vicinity of its source satellites) where the impact ionization detector of the CDA is saturated.
5. J. H. Waite Jr. *et al.*, *Science* **311**, 1419 (2006).
6. C. J. Hansen *et al.*, *Science* **311**, 1422 (2006).
7. M. K. Dougherty *et al.*, *Science* **311**, 1406 (2006).
8. Early decoupling of gas and dust is in accordance with the reported low gas densities [Knudsen regime (*5*)] found in the gas plume (*6*), making molecule-dust collisions unlikely during the time (tens of minutes) from ejection to the impact of the grain at the HRD.
9. J. R. Spencer *et al.*, *Science* **311**, 1401 (2006).
10. H. Krüger, A. V. Krivov, D. P. Hamilton, E. Grün, *Nature* **399**, 558 (1999).
11. P. K. Haff, G. L. Siscoe, A. Eviatar, *Icarus* **56**, 426 (1983).
12. J. S. Kargel, S. Pozio, *Icarus* **119**, 385 (1996).
13. J. E. Colwell, *Icarus* **106**, 536 (1993).
14. M. Sremčević, A. V. Krivov, H. Krüger, F. Spahn, *Planet. Space Sci.* **53**, 625 (2005).
15. C. C. Porco *et al.*, *Science* **311**, 1393 (2006).
16. Within the Hill sphere, the satellite's gravity dominates Saturn's gravity. The Hill radius is defined in terms of the masses of Saturn M_S and Enceladus M_E, and of the distance a_E between them, as $r_h = a_E \sqrt[3]{M_E/3(M_S + M_E)}$.
17. M. Sremčević, A. V. Krivov, F. Spahn, *Planet. Space Sci.* **51**, 455 (2003).
18. Materials and methods are available as supporting material on *Science* Online.
19. Perturbation forces (Saturn's oblateness, Lorentz force, and radiative forces) are crucial for the long-term dynamics of the particle and the configuration of the E ring (*22*–*26*). They can be neglected for the simulation of dust in the vicinity of Enceladus.
20. A. V. Krivov, M. Sremčević, F. Spahn, V. V. Dikarev, K. V. Kholshevnikov, *Planet. Space Sci.* **51**, 251 (2003).
21. Initial velocities follow a cumulative power law $N\,(>v) \propto v^{-2}$, $0.15\ v_{esc} < v < 2\ v_{esc}$, where $v_{esc} \sim 239$ m s^{-1} is Enceladus' escape velocity. Starting directions are uniformly distributed in a cone of semi-opening angle of 25° normal to the surface at the starting location.
22. M. Horányi, J. A. Burns, D. P. Hamilton, *Icarus* **97**, 248 (1992).
23. D. P. Hamilton, J. A. Burns, *Science* **264**, 550 (1994).
24. V. V. Dikarev, *Astron. Astrophys.* **346**, 1011 (1999).
25. F. Spahn, K.-U. Thiessenhusen, J. Colwell, R. Srama, E. Grün, *J. Geophys. Res.* **104**, 24111 (1999).
26. A. Juhász, M. Horányi, *Geophys. Res. Lett.* **31**, 19703 (2004).

27. We thank T. V. Johnson for comments on the manuscript. The Potsdam group was supported by Deutsche Forschungsgemeinschaft grants Sp 384/16, Sp 384/17, and Sp 384/18; Deutsches Zentrum für Luft und Raumfahrt (DLR) grant 50OH0003; and the Studienstiftung des deutschen Volkes. The group at the Max Planck Institut für Kernphysik was supported by the Max Planck Society and by DLR under grant 50OH9802. The work in Chicago was supported by Jet Propulsion Laboratory contract 96 11 70, and M. Sremčević is funded by the Cassini UVIS project.

Supporting Online Material

www.sciencemag.org/cgi/content/full/311/5766/1416/DC1
Materials and Methods
Figs. S1 to S7
References

14 October 2005; accepted 19 January 2006
10.1126/science.1121375

Downloaded from www.sciencemag.org on October 24, 2007